View Article Online
View Journal

Dalton Transactions

An international journal of inorganic chemistry

Accepted Manuscript

This article can be cited before page numbers have been issued, to do this please use: J. J. Mihaly, D. J. Stewart, T. Grusenmeyer, A. Phillips, J. E. Haley, M. Zeller and T. Gray, *Dalton Trans.*, 2019, DOI: 10.1039/C9DT02312G.

This is an Accepted Manuscript, which has been through the Royal Society of Chemistry peer review process and has been accepted for publication.

Accepted Manuscripts are published online shortly after acceptance, before technical editing, formatting and proof reading. Using this free service, authors can make their results available to the community, in citable form, before we publish the edited article. We will replace this Accepted Manuscript with the edited and formatted Advance Article as soon as it is available.

You can find more information about Accepted Manuscripts in the Information for Authors.

Please note that technical editing may introduce minor changes to the text and/or graphics, which may alter content. The journal's standard Terms & Conditions and the Ethical guidelines still apply. In no event shall the Royal Society of Chemistry be held responsible for any errors or omissions in this Accepted Manuscript or any consequences arising from the use of any information it contains.

ROYAL SOCIETY OF CHEMISTRY

rsc.li/dalton

View Article Online
DOI: 10.1039/C9DT02312G

Photophysical Properties of Organogold(I) Complexes Bearing a Benzothiazole-2,7-Fluorenyl Moiety: Selection of Ancillary Ligand Influences White Light Emission

Joseph J. Mihaly,[a] David J. Stewart,[b,c] Tod A. Grusenmeyer,[b] Alexis T. Phillips,[b,d] Joy E. Haley,[b] Matthias Zeller,[e] and Thomas G. Gray[a,*]

[a]Department of Chemistry, Case Western Reserve University, 10900 Euclid Avenue, Cleveland, Ohio 44106, United States

[b]Air Force Research Laboratory, Materials and Manufacturing Directorate, Wright-Patterson Air Force Base, Dayton, Ohio 45433, United States

[c]General Dynamics Information Technology, 5000 Springfield Pike, Dayton, Ohio, 45431, United States

[d]Southwestern Ohio Council for Higher Education, Dayton, Ohio, 45420, United States

[e]Department of Chemistry, Purdue University, West Lafayette Indiana, 47907, United States

Keywords: Gold, dual luminescence, white light emission, long-lived triplet excited states, triplet-triplet annihilation, excited-state absorption, crystal structure

View Article Online
DOI: 10.1039/C9DT02312G

Abstract.

Herein we report three new gold(I) complexes with a benzothiazole-2,7-fluorenyl moiety bound through a gold-carbon σ-bond and either an *N*-heterocyclic carbene or organophosphine as ancillary ligands. The complexes have been characterized by NMR spectroscopy, X-ray crystallography, high resolution mass spectrometry, elemental analysis, and static and time-resolved optical spectroscopy. These compounds absorb almost strictly in the ultraviolet region and exhibit dual-luminescence following three freeze-pump-thaw cycles in toluene. The selection of the ancillary ligand significantly influences the excited-state dynamics of the complexes. The two phosphine containing complexes have similar fluorescence and phosphorescence quantum yields leading to generation of white light emission. The carbene containing complex exhibits a higher fluorescence quantum yield compared to its phosphorescence quantum yield resulting in a violet emission. Extensive photophysical characterization of these compounds suggests that the phosphine complexes undergo intersystem crossing more efficiently than the carbene complex. This is supported by a three-fold increase in luminescence lifetime, a halving in fluorescence quantum yield, and an increase in intersystem crossing efficiency by 25 percent for the phosphine complexes. Density-functional theory calculations support these observations where the energy gap between the S_1 and T_2 states for the carbene is roughly twice that of the phosphine complexes. To our knowledge this is the first example of single-component mononuclear gold(I) complexes exhibiting non-excimeric state white light emission, although a similar phenomenon has been realized for gold(III) aryl compounds. Further, the triplet lifetimes of all three complexes are on the order of one ms in freeze-pump-thaw degassed toluene. These molecules also exhibit delayed fluorescence; all of the complexes display diffusion-controlled rate constants for triplet-triplet annihilation. Strong excited-state absorption is observed from the singlet and triplet excited-states in these molecules as well. The singlet states have excited-state extinction coefficients on the order of 1.5×10^5 M^{-1} cm^{-1} and the triplet states have excited-state extinction coefficients on the order of 1.0×10^5 M^{-1} cm^{-1}.

View Article Online
DOI: 10.1039/C9DT02312G

Introduction

Late d-block σ-organometallics have received sustained attention for excited-state properties that come about, in part, through the heavy-atom effect.[1–7] When a heavy metal is covalently embedded in a conjugated organic chromophore, long-lived triplet excited states can be populated owing to the metal's spin-orbit coupling.[8,9]. The resulting complexes are phosphorescence emitters, often with radiative lifetimes in the microsecond range near 200 K. Potential applications include oxygen sensing,[10–12] photodynamic therapy,[13,14] solar energy harvesting,[15,16] light-emitting diode construction,[17–31] low-power upconversion,[32–34] and nonlinear optics.[35–38]

More specifically, organometallic complexes have been extensively researched as chromophores for organic light-emitting diodes (OLEDs) both as colored displays and white light emitting materials for use in solid-state lighting technology (WOLEDs).[39–48] Currently, two techniques are applied to generate white light and both are multicomponent: The first is a combination of red, green, and blue emission and the second employs use of complimentary emission such as blue and orange.[49–55] This leads to an often-complicated device fabrication/doping process to produce white light; a severely understudied, yet proposed alternative is to generate white light from a single entity eliminating the need for a multi-emitter system.[56,57]

Several studies have emerged in an effort to realize single-component coordination compounds that emit white light both in solution and the solid state. The pursuit for such compounds has encompassed transition metal small molecules to heavy metal containing polymers. Much work on this problem has focused on platinum(II) and iridium(III) species. In 2006, Cao and co-workers realized a true single-component white emitter from two different iridium(III) based polymeric systems.[58,59] Both systems were achieved by a combination of incorporating red, blue, and green emitting chromophores into the same polymeric backbone as well as combining dual fluorescence and phosphorescence emitters to span the visible region. Both polymers demonstrated white emission through both photoluminescence and electroluminescence.

Platinum(II) compounds have also been achieved as single-component white emitters. In 2016, Venkatesan and co-workers synthesized a variety of platinum(II) alkynyl compounds that demonstrated white light emission through combining monomeric and eximeric states to produce

View Article Online
DOI: 10.1039/C9DT02312G

high energy blue and lower energy orange emission simultaneously in a poly(methyl methacrylate) (PMMA) matrix.[60]

Gold(I) and gold(III) complexes, though understudied, have also been explored. Li and co-workers synthesized a trinuclear gold(I) cluster that achieved white light emission by regulating aggregation.[61] It was deemed that the emission color could be tuned ultimately from monomer-excimer equilibria where the excimer formation is facilitated by aurophilic interactions. Lastly, in 2017 Venkatesan and co-workers synthesized four gold(III) aryl complexes, where three are white light emitters by CIE 1931 coordinates in dichloromethane solution and somewhat less so in PMMA films.[62] Venkatesan and co-workers demonstrated that white light emission can be achieved by combining blue fluorescence with orange phosphorescence to yield emission covering the visible spectrum, and therefore attaining white light in complexes of gold(III). Here, we describe the synthesis, structural authentication, and optical characterization of mononuclear gold(I) complexes of benzothiazolyl-substituted fluorophores. Ancillary ligands on gold are organophosphines and an *N*-heterocyclic carbene. We show that attachment of a single gold center generates dual (singlet and triplet) luminescence. The organophosphine-containing complexes exhibit dual luminescence with comparable fluorescence and phosphorescence quantum yields, generating white light emission. Complete photophysical characterization by static and time-resolved optical spectroscopy is described within.

Results and Discussion

Reaction of the known[63] (pinacolato)boron ester with (phosphine)gold(I) bromide or (*N*-heterocyclic carbene)gold(I) chloride[64–69] at 55 °C afforded the corresponding (aryl)gold(I) species **AuBTF0** (72 % yield), **AuBTF1** (76 % yield), and **AuBTF2** (53 % yield), Scheme 1, which were isolated by vapor diffusion of pentane into concentrated dichloromethane solutions, to afford diffraction-quality crystals. The new compounds are stable to ambient air and lighting, with melting points of 223 °C (**AuBTF0**), 233 °C (**AuBTF1**), and 241 °C (**AuBTF2**). A thermal ellipsoid depiction of **AuBTF1**, which is representative, appears as Figure 1. The gold-aryl-carbon bond length of **AuBTF1** is 2.0498(16) Å; the gold-phosphorus distance is 2.2950(4) Å, and the phosphorus-gold-carbon angle is 177.63(5). These metrics are typical for complexes of gold(I).[65,68,70–72] Metrics of the BTF ligand are unexceptional. The crystal structures of **AuBTF0**

View Article Online
DOI: 10.1039/C9DT02312G

and **AuBTF2** appear in the supporting information, along with geometric data for all three compounds. Aurophilic interactions are not evident in any structure, with the closest approach of gold atoms (in **AuBTF1**) exceeding 7.6 Å. None of the three structures shows evidence for π-stacking of aryls. Synthetic procedures and structural characterization, including NMR and combustion analysis data, can be found in the ESI.

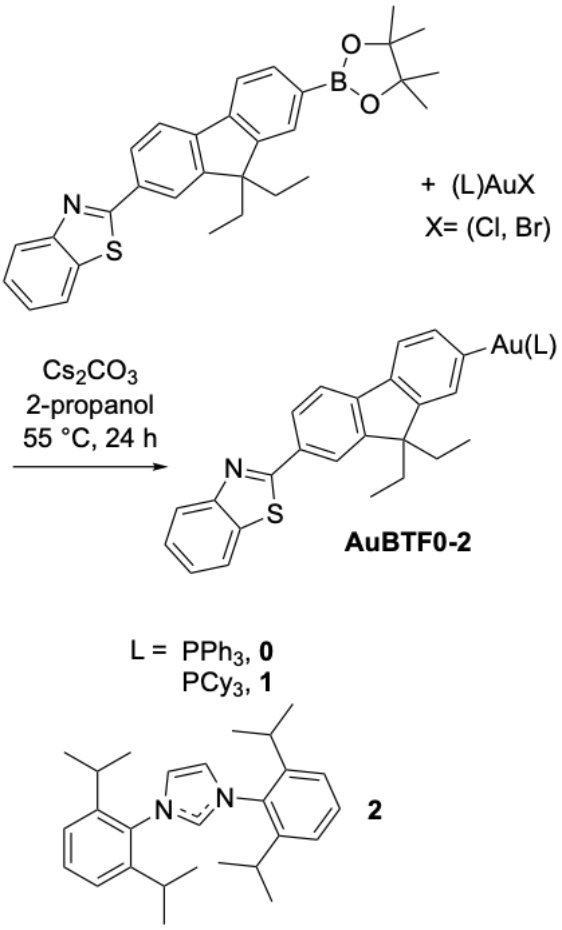

Scheme 1. Syntheses of gold(I) complexes of this study.

View Article Online
DOI: 10.1039/C9DT02312G

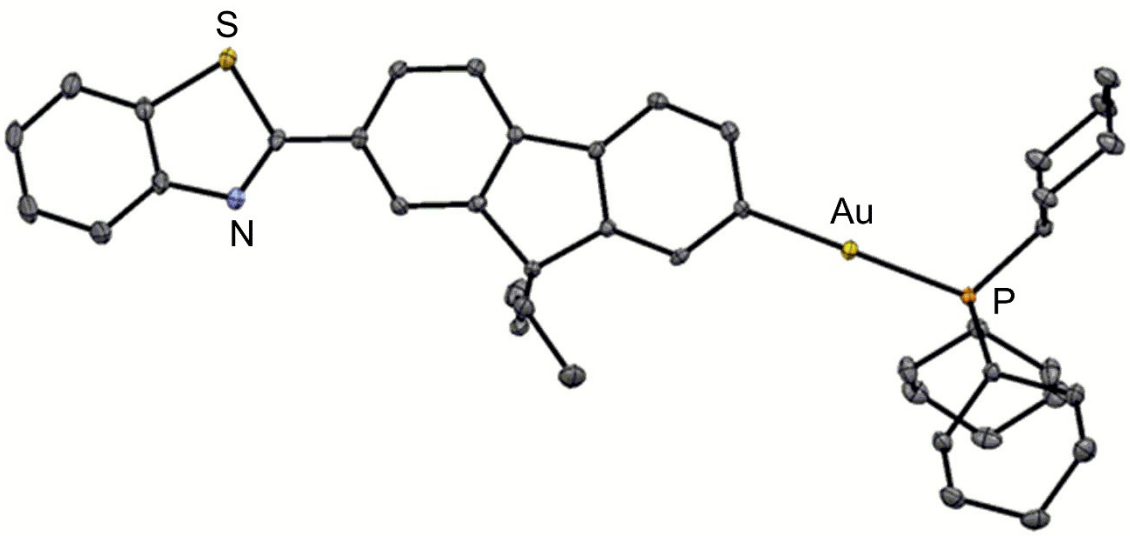

Figure 1. Thermal ellipsoid representation of **AuBTF1** (50% probability level, 150 K). Hydrogen atoms are omitted for clarity. Unlabeled atoms are carbon.

Ground-state absorption and luminescence spectroscopy. The ground-state absorption spectra in molar absorptivity units are in shown in Figure 2. The normalized dual emission spectra obtained following three freeze-pump-thaw cycles in toluene and the corresponding CIE 1931 chromaticity diagram are

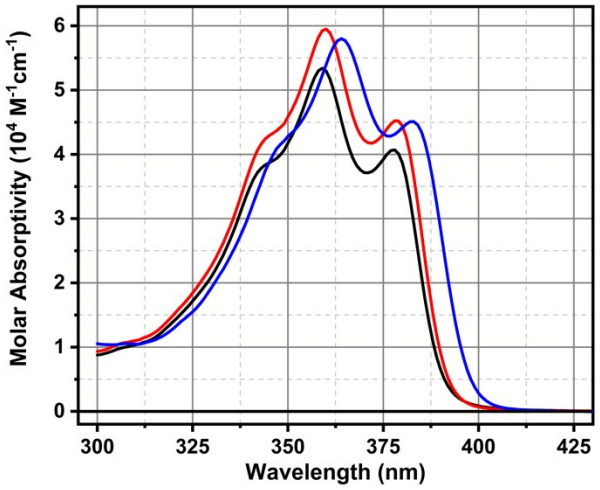

Figure 2. Ground-state absorption spectra of **AuBTF0** (black), **AuBTF1** (red), and **AuBTF2** (blue) collected in toluene.

shown in Figure 3. Pertinent wavelength and ground-state extinction coefficient values are reported in Table 1. The spectral band shapes of the ground-state absorption spectra are identical

View Article Online
DOI: 10.1039/C9DT02312G

for all complexes. They are characterized by two well-resolved absorption maxima at wavelengths longer than 350 nm and a high-energy shoulder at approximately 340 nm. The observation of highly structured ground-state absorption spectra implies that these transitions are ππ* in nature. The energies of the absorption transitions are controlled by the ancillary ligand attached to the Au(I) atom. The two phosphine containing complexes have absorption transitions that occur at nearly identical energies with maxima occurring at 359 nm for **AuBTF0** and 360 nm for **AuBTF1**. The installation of the *N*-heterocyclic carbene ligand results in a slight bathochromic shift resulting in an **AuBTF2** absorption maximum at 364 nm. The ground-state extinction coefficients are similar for the complexes; all have values on the order of 5 x 10^4 M^{-1} cm^{-1}. The emission spectra following three freeze-pump-thaw cycles in toluene are characterized by dual luminescence. The spectral band shapes of the observed fluorescence and phosphorescence emissions from all of the complexes are indistinguishable and highly structured; the vibronic structure suggests ππ* character of the underlying emission. Fluorescence and phosphorescence maxima follow the same energetic ordering as the ground-state absorption maxima: **AuBTF0** ≈ **AuBTF1** > **AuBTF2.** The fluorescence and phosphorescence energies of the complexes are similar with the respective energies of **AuBTF0**, **AuBTF1**, and **AuBTF2** all occurring within 10 nm of one another. The presence of dual luminescence indicates that intersystem crossing to form the triplet state competes with radiative and non-radiative decay from the excited singlet state. Fluorescence and phosphorescence lifetime (Figure S10), fluorescence quantum yield (Figure S11), phosphorescence quantum yield (Figure S12), and intersystem crossing quantum yield (Figure S13) experiments were all performed in toluene to gain insight into the excited-state dynamics. The results of these experiments are summarized in Table 1. The detailed procedures used in the collection of these data are provided in the ESI. **AuBTF0** and **AuBTF1** display nearly identical fluorescence and intersystem crossing behavior. Their fluorescence lifetimes are both on the order of 90 ps, their fluorescence quantum yield values are essentially 0.10, and their intersystem crossing quantum yields are approximately 0.80. On the other hand, **AuBTF2** has a fluorescence lifetime of 229 ps, a fluorescence quantum yield of 0.22, and an intersystem crossing yield of 0.63. Changing the ancillary ligand in these complexes from a phosphine to an *N*-heterocyclic carbene changes the luminescence lifetime by a factor of three, the fluorescence quantum yield by a factor

View Article Online
DOI: 10.1039/C9DT02312G

of two, and lowers the intersystem crossing efficiency by twenty-five percent. The combination of these lifetime and quantum yield results allows for the determination of the radiative (k_r), non-radiative (k_{nr}), and intersystem crossing (k_{isc}) rate constants. Predictably, the values of k_r, k_{nr}, and k_{isc} for **AuBTF0** and **AuBTF1** are equivalent. Intersystem crossing is the dominant kinetic pathway in **AuBTF0** and **AuBTF1** with a rate constant of 9×10^9 s^{-1}. This is an order of magnitude greater than the rate constants for radiative and non-radiative decay in these complexes. The kinetic behavior of **AuBTF2** is remarkably different. Intersystem crossing is still the dominant kinetic pathway in this complex but its rate constant is about four times less than in **AuBTF0** and **AuBTF1**. Not only is the rate of intersystem crossing diminished in **AuBTF2** but the magnitude of k_{nr} is roughly two times smaller than in **AuBTF0** and **AuBTF1**. The phosphorescence quantum yield is less sensitive to structural variations in these molecules, with similar values of approximately 0.10. The combination of the diminished rates of intersystem crossing and non-radiative decay in **AuBTF2** and the similar values for the phosphorescence quantum yields across the series of AuBTF complexes has direct implications on the white light emission behavior of these complexes. In **AuBTF0** and **AuBTF1**, the fluorescence and phosphorescence quantum yields are similar; the resulting dual emission appears white. In **AuBTF2**, the fluorescence quantum yield is a factor of two larger than the phosphorescence quantum yield, and the resulting emission appears violet in color. This change in the luminescence color is demonstrated in the inset of Figure 3 and CIE 1931 chromaticity diagram.

Phosphorescence Lifetimes. Due to the efficient phosphorescence in these systems, we were also able to collect phosphorescence lifetimes. The complexes all possess phosphorescence lifetimes on the order of 1 ms following three freeze-pump-thaw cycles in toluene. It should be noted that the observed lifetime is highly dependent upon the lowest vacuum pressure achieved during the freeze-pump-thaw deaeration cycles. Vacuum pressures of less than 100 mTorr are achieved using our evacuation set-up. This corresponds to oxygen concentrations of approximately 1 μmol. The Stern-Volmer relationship can be used to evaluate the magnitude of excited-state quenching under these conditions. The Stern-Volmer relationship is shown in Equation 1,[73]

$$\frac{\tau_0}{\tau} = 1 + k_q \tau_0 [Q], \quad (1)$$

View Article Online
DOI: 10.1039/C9DT02312G

where τ_0 is the freeze-pump-thaw deaerated lifetime of the complex, τ is the lifetime in the presence of oxygen, k_q is the bimolecular quenching constant, [Q] is the concentration of dissolved oxygen in the solution. A vast majority of charge neutral organic molecules have k_q values on the order of 1 x 10^{10} and 1 x 10^9 $M^{-1}s^{-1}$.[74] The oxygen concentration in the cell can be estimated using the ideal gas law. There are 4.85 μmoles of gas present in a 1 L liter vessel at standard temperature with a pressure of 90 mTorr. We assume the gas has a composition of 20% oxygen. An oxygen concentration of 1 μM is reasonable under our cell conditions. Evaluation of the Stern-Volmer equation using a phosphorescence lifetime value of 1 ms, the estimated oxygen concentration value of 1 μM and bimolecular quenching constants of 1 x 10^{10} and 1 x 10^9 $M^{-1}s^{-1}$ return τ_0/τ values of 11 and 2, respectively. This numerical treatment of these data accentuates the sensitivity of the solution lifetime values to the final pressure in the freeze-pump-thaw cell. It should further be noted that the lifetime value obtained in solution may not reflect the intrinsic lifetime of the chromophore but the maximum obtainable lifetime value at the given oxygen concentration, particularly for chromophores with very long triplet lifetimes. With this in mind, the lowest achieved vacuum pressure in the freeze-pump-thaw degassed cycles is recorded along with the reported phosphorescence lifetime. This vacuum pressure was replicated for all subsequent measurements where freeze-pump-thaw deaeration was utilized.

View Article Online
DOI: 10.1039/C9DT02312G

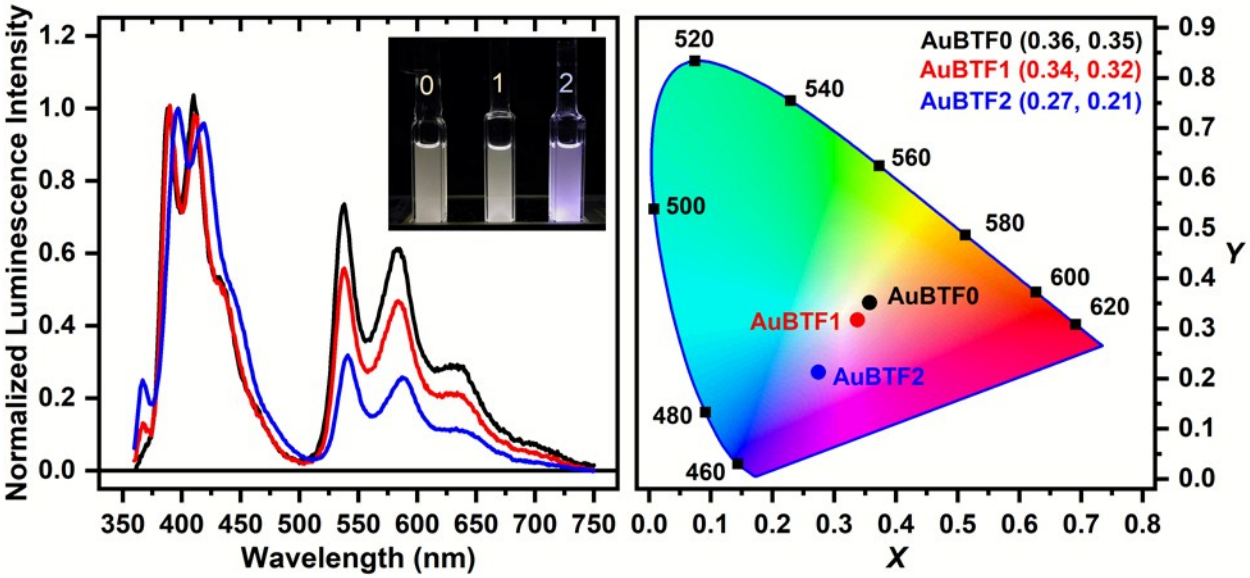

Figure 3. Normalized dual emission spectra (left) and CIE 1931 chromaticity diagram (right) **AuBTF0** (black), **AuBTF1** (red), and **AuBTF2** (blue) following three freeze-pump-thaw cycles in toluene. Inset: Image of luminescence from freeze-pump-thaw deaerated samples of the complexes. The cuvettes are on the surface of a UV hand lamp and being irradiated from the bottom of the cell.

View Article Online
DOI: 10.1039/C9DT02312G

Table 1. Summary of AuBTF Photophysical Properties

Complex	AuBTF0	AuBTF1	AuBTF2
λ_{ABS}/nm (10^4 $M^{-1}cm^{-1}$)	359 (5.34 ± 0.68)	360 (5.95 ± 0.18)	364 (5.80 ± 0.18)
[A]λ_{FL} (nm)	388	389	397
ϕ_{FL}	0.08 ± 0.01	0.09 ± 0.03	0.22 ± 0.01
τ_{FL} – TCSPC (ps)	79.3	89.4	229
τ_{FL} – TA (ps)	84.5 ± 4.6	95.4 ± 2.3	279 ± 10
k_r (s^{-1})	9.4 x 10^8	9.5 x 10^8	7.9 x 10^8
k_{nr} (s^{-1})	1.5 x 10^9	1.1 x 10^9	5.4 x 10^8
k_{ISC} (s^{-1})	9.3 x 10^9	8.5 x 10^9	2.3 x 10^9
[B]λ_{PHOS} (nm)	538	538	541
$\phi_{TRIPLET}$	0.79 ± 0.01	0.81 ± 0.02	0.63 ± 0.03
ϕ_{PHOS}	0.09 ± 0.01	0.07 ± 0.01	0.11 ± 0.01
τ_{PHOS} (μs) *Vac. Pressure (mTorr)*	810 ± 70 *89*	766 ± 8 *90*	872 ± 59 *87*
k_T (s^{-1})	1220	1290	1140
k_{TT} ($M^{-1}s^{-1}$)	1.3 ± 0.1 x 10^{10}	1.2 ± 0.1 x 10^{10}	1.4 ± 0.1 x 10^{10}
$\Delta\varepsilon_{T_1-T_n}$/λ nm ($10^4$ M^{-1} cm^{-1})	547 (9.14 ± 0.50)	550 (10.1 ± 0.1)	562 (9.40 ± 0.10)
$\Delta\varepsilon_{S_1-S_n}$/λ nm ($10^4$ M^{-1} cm^{-1})	567 (13.7)	588 (15.6)	557 (15.0)

All Data collected in room temperature toluene. Legend: λ_{FL} = wavelength of fluorescence; ϕ_{FL} = emission quantum yield of fluorescence; τ_{FL} = lifetime of fluorescence; TCSPC = time-correlated single-photon counting; TA = transient absorption; k_r = radiative decay rate constant; k_{nr} = nonradiative decay rate constant; k_{ISC} = rate constant of intersystem crossing; λ_{PHOS} = wavelength of phosphorescence; $\phi_{TRIPLET}$ = quantum yield of triplet state formation; ϕ_{PHOS} = emission quantum yield of phosphorescence; τ_{PHOS} = lifetime of phosphorescence; k_T = rate constant for formation of triplet excited state; k_{TT} = rate constant of triplet-triplet annihilation; $\Delta\varepsilon_{T_1-T_n}$= molar absorptivity of triplet-triplet absorption; $\Delta\varepsilon_{S_1-S_n}$ = molar absorptivity of excitied-singlet-singlet absorption.

[A]Estimated from the peak maximum of the dilute luminescence spectrum used for the reabsorption correction in fluorescence quantum yield experiments (Figure S2).

[B]Estimated from the peak maximum of the phosphorescence signal shown in Figure 3.

Nanosecond transient absorption spectroscopy and delayed fluorescence. Nanosecond transient absorption difference spectra of all three complexes in units of Δε (the difference between the excited and ground-state extinction coefficients) vs. wavelength are shown in Figure 4. The

View Article Online
DOI: 10.1039/C9DT02312G

values of Δε for each of the chromophores are given in Table 1. The spectra

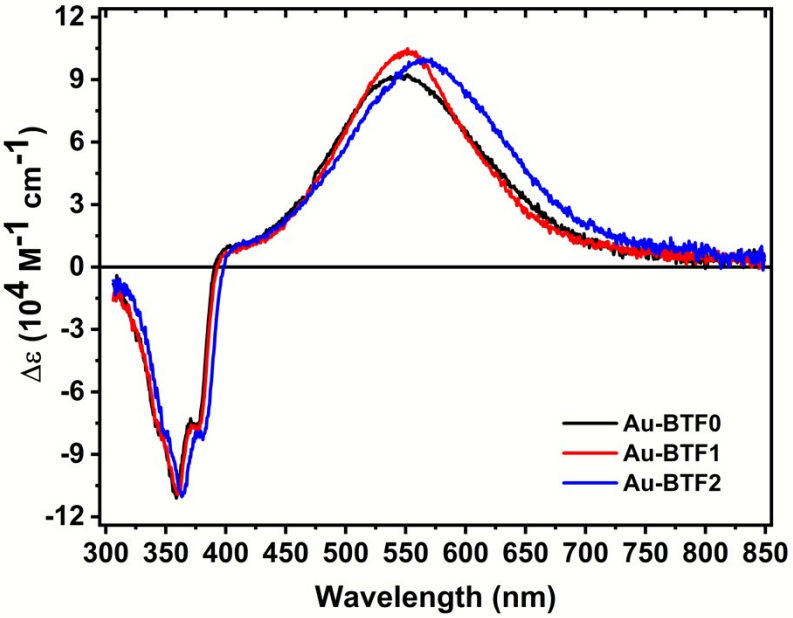

Figure 4. Nanosecond transient absorption difference spectra of **AuBTF0** (black), **AuBTF1** (red), and **AuBTF2** (blue) collected following three freeze-pump-thaw cycles in toluene. All samples were excited at 355 nm. The spectra were collected 100 ns after the laser pulse. Spectra were converted to units of Δε using relative actinometry measurements with a $[Ru(bpy)_3]^{2+}$ standard (see Materials and Methods in SI).

were collected and converted from units of ΔOD to units of Δε using $[Ru(bpy)_3]^{2+}$ as a relative actinometer. This method is described in detail in the Supporting Information. The data used to calculate the values of Δε are shown in Figure S16. The nanosecond transient absorption spectra are characterized by a bleach of all of the ground-state absorption features below 400 nm with broad positive absorption from 400 – 800 nm. The maxima of the positive absorption features are slightly different for the three complexes. The observed maximum in the triplet-triplet absorption spectrum is similar for **AuBTF0** and **AuBTF1** but is slightly red-shifted for **AuBTF2**. The triplet states of all of the AuBTF complexes possess strong excited-state absorption; the excited-state extinction coefficients ($\Delta\varepsilon_{T_1-T_n}$) for all three molecules are on the order of 1 x 10^5 M^{-1} cm^{-1}. Initial kinetic decay traces were collected for the molecules at the maximum of the positive excited-state absorption feature. The data show that an increase in laser pulse energy results in an increase in the initial rate of excited-state decay. Delayed fluorescence is also observed in these complexes.

View Article Online
DOI: 10.1039/C9DT02312G

This combination of laser-energy-dependent kinetic behavior and delayed fluorescence implies that triplet-triplet annihilation contributes to the deactivation of the triplet excited-states.[75] To this end, the influence of incident laser pulse energy on the integrated delayed fluorescence intensity was explored. Plots of the delayed luminescence signal obtained at various incident laser pulse energies are shown in Figure S14. The luminescence intensity at each laser power is normalized to the maximum of the phosphorescence signal in order to demonstrate the effect of variations in the laser pulse energy on the observed delayed fluorescence intensity. A plot of the normalized delayed fluorescence intensity vs. the incident laser pulse energy for **AuBTF0** is shown in Figure 5. The fit line represents the best quadratic fit of the data. The double logarithm plot of this data is shown in the inset. The slope of the linear fit of the log data is 1.69. The slope of this fit should be equal to 2 if the delayed fluorescence is the result of triplet-triplet annihilation.[75] The corresponding data for **AuBTF1** and **AuBTF2** are shown in Figure S15. Interestingly, the linear fits of the log plots for **AuBTF1** and **AuBTF2** also return slope values significantly less than 2 with values of 1.66 and 1.80, respectively. We believe this discrepancy between the observed and expected slope values to be due to the fast and efficient intersystem crossing in these AuBTF complexes discussed above. This causes the conversion of a significant number of the upconverted singlets back to the triplet state, resulting in a lower than expected integrated delayed fluorescence signal. This is supported by the fact that **AuBTF0** and **AuBTF1** ($k_{isc} \sim 9 \times 10^9$) have lower slope values than **AuBTF2** ($k_{isc} \sim 2 \times 10^9$).

View Article Online
DOI: 10.1039/C9DT02312G

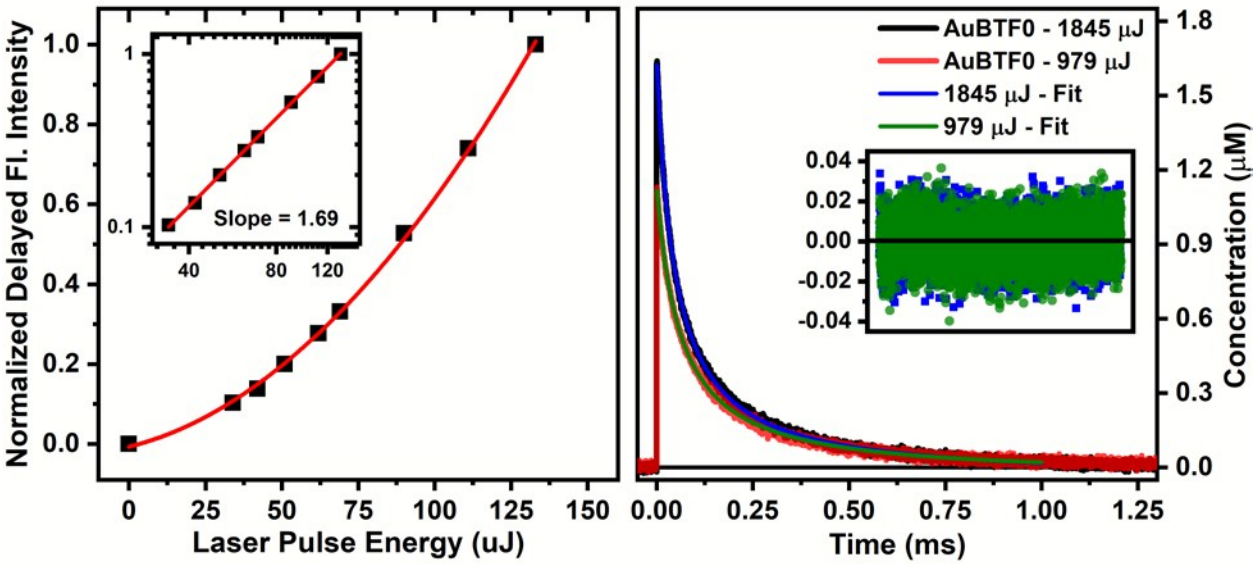

Figure 5. (Left) Plot of the normalized, integrated fluorescence intensity vs. laser pulse energy for a sample of **AuBTF0** following three freeze-pump-thaw cycles in toluene. The fit line represents the best quadratic fit of the data. The double logarithm plot of the same data is inset with the slope obtained from a linear fit listed. (Right) Triplet-triplet annihilation fitting of excited-state decay traces of **AuBTF0** in freeze-pump-thaw deaerated toluene. The inset depicts the residuals of both data fits.

The rate constants for triplet-triplet annihilation (k_{TT}) can be determined by the fitting kinetic decay traces obtained from nanosecond transient absorption measurements following the conversion of the data from units of ΔOD to concentration.[75] A detailed discussion of this process and the fit equation are provided in the ESI. Excited-state decay traces obtained from **AuBTF0** in toluene at two different laser energies and the corresponding triplet-triplet annihilation fits are shown in Figure 5. The residuals for the fits are displayed in the inset. The fits of excited-state decay traces for **AuBTF1** and **AuBTF2** are shown in Figure S15. The values for k_{TT} obtained from the representative fits of the decay traces are reported in Table 1. All of the datasets are fit well using this kinetic treatment. For all three chromophores, the rate constant for triplet-triplet annihilation is on the order of 1×10^{10} M^{-1} s^{-1}. This value approaches the diffusion limit in toluene[74], signifying that triplet-triplet annihilation is a diffusion controlled process in these AuBTF complexes in toluene at room temperature.

View Article Online
DOI: 10.1039/C9DT02312G

Picosecond transient absorption measurements. Picosecond transient absorption measurements were used to investigate the absorption properties of the singlet excited-state and

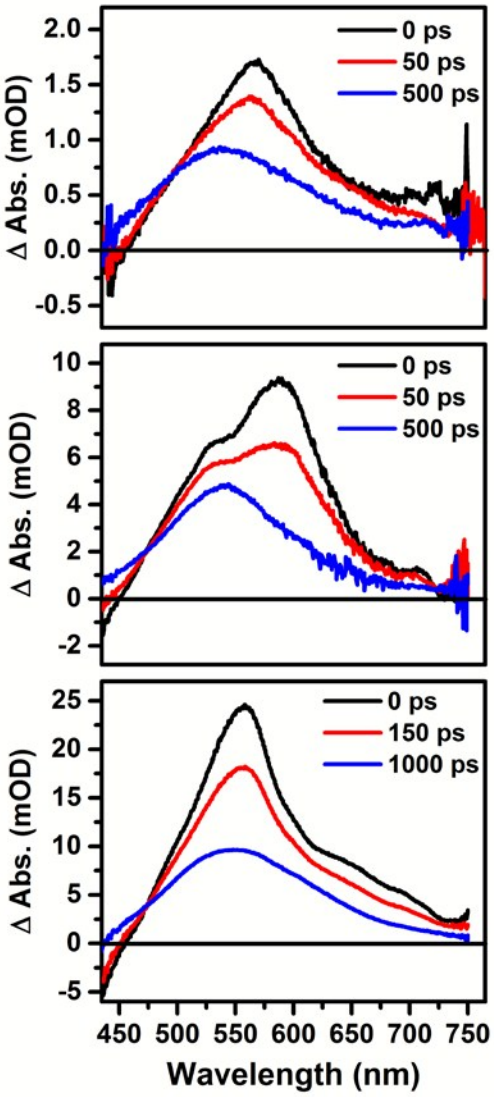

Figure 6. Picosecond transient absorption difference spectra collected at various time delays (see inset) for (top) **AuBTF0**, (middle) **AuBTF1**, and (bottom) **AuBTF2** in aerated toluene. All samples were excited using the frequency doubled output of Ti:sapphire.

the evolution from the singlet excited-state to the triplet excited-state. The picosecond transient absorption difference spectra of all three complexes are shown in Figure 6. Representative monoexponential fits of single wavelength kinetic decay traces collected in these experiments are shown in Figure S17. The singlet lifetime values obtained from these picosecond transient absorption experiments are presented in Table 1. The values given in Table 1 are the average of

View Article Online
DOI: 10.1039/C9DT02312G

the lifetimes at 10 unique wavelengths in the transient absorption spectrum using the Surface Xplorer software. The $S_1 - S_n$ absorption transitions are represented by the 0 ps spectra and $T_1 - T_n$ absorption transitions are represented by the 500 ps spectra for **AuBTF0** and **AuBTF1** and the 1000 ps spectrum for **AuBTF2** in Figure 6. The picosecond transient absorption spectra are dominated by positive transient absorption from 450 – 750 nm. The $S_1 \rightarrow S_n$ absorption transitions are particularly strong; their transient absorption signals are about two times greater than the signal corresponding to the $T_1 \rightarrow T_n$ transitions. The previously determined values of $\Delta\varepsilon_{T_1-T_n}$ and $\phi_{TRIPLET}$ allow for the determination of the singlet excited-state extinction coefficient ($\Delta\varepsilon_{S_1-S_n}$) values. A detailed discussion of this process is included in the Supporting Information. The calculated values are reported in Table 1. All three AuBTF complexes have $\Delta\varepsilon_{S_1-S_n}$ values on the order of 1.5 x 10^5 M^{-1} cm^{-1}. In all of the complexes, the progression from the singlet excited-state to the triplet excited-state is well-represented with a single exponential decay kinetic model and the presence of a single isosbestic point at ≈ 475 nm. There is no evidence of fast kinetic components corresponding to internal conversion (IC) or intramolecular vibrational energy redistribution (IVR). The lifetime values obtained from fits of the picosecond transient absorption kinetic decay traces are in good agreement with the fluorescence lifetime values obtained in TCSPC experiments.

Calculations

Density-functional theory calculations were performed to analyze the bonding and Franck-Condon excited states of **AuBTF1** and **AuBTF2**. Geometries were fully optimized starting from the crystal structures of both compounds; harmonic vibrational frequency calculations revealed the converged structures to be minima of the potential energy hypersurfaces. Computed metrics are in good agreement with crystallographic values. All calculations proceeded with a continuum dielectric treatment of toluene solvation.

Figure 7 depicts a frontier orbital energy level diagram of **AuBTF1** along with plots of selected orbitals. The highest occupied Kohn-Sham orbital (HOMO) is delocalized over the entire carbanionic ligand, with only small contributions from (phosphine)gold(I) moiety. These results concur with the observed vibronic structure in the emission spectra of all three complexes, which indicates that the transitions are ππ* in nature. The diethylfluorenyl moiety accounts for some 79%

View Article Online
DOI: 10.1039/C9DT02312G

of electron density of the HOMO; the benzothiazolyl contributes 17%. Density in the lowest unoccupied Kohn-Sham orbital (LUMO) is 50% localized on the fluorenyl, with 48% on the benzothiazolyl. The tricyclohexylphosphine ligand is optically innocent, and contributes 0.5% (of density) to both HOMO and LUMO.

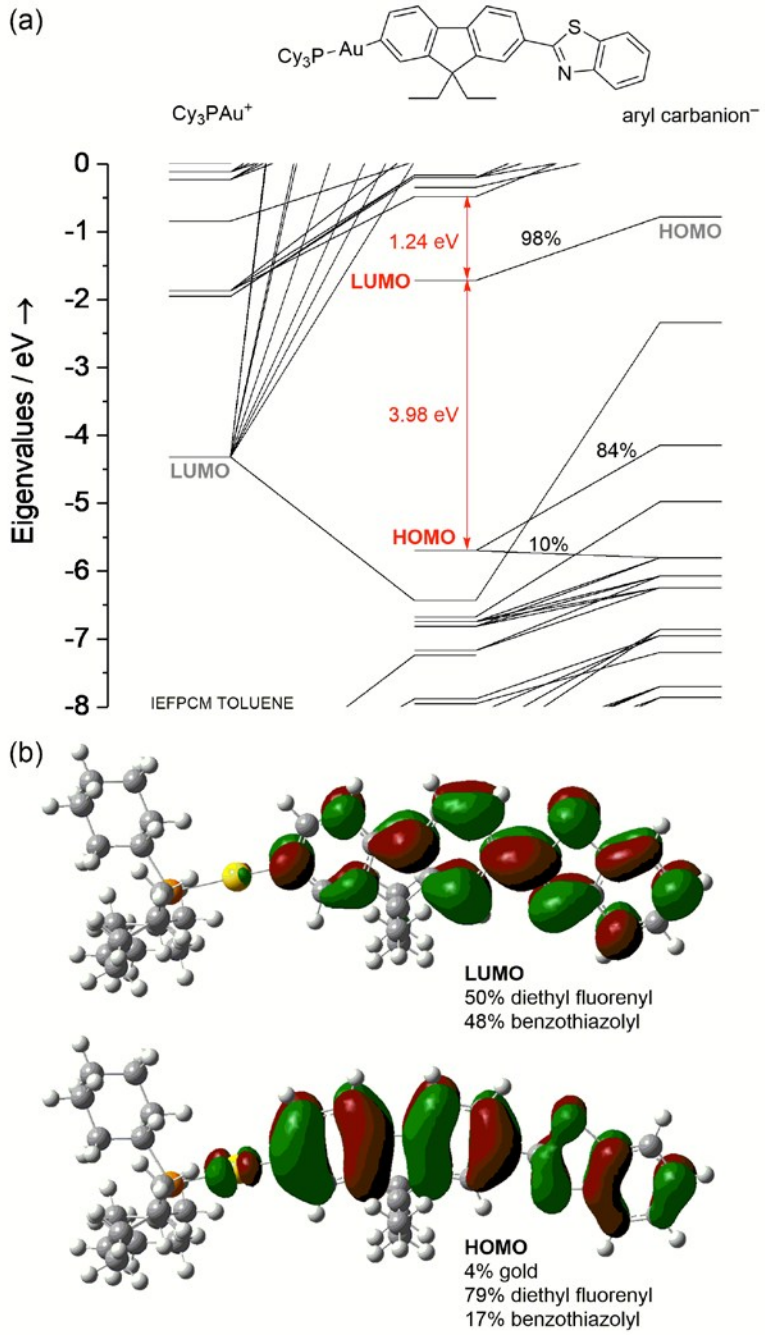

Figure 7. (a) Frontier orbital energy level diagram of **AuBTF1**. (b) Plots of frontier Kohn-Sham orbitals (HOMO) and (LUMO) (Percentages are of electron density).

View Article Online
DOI: 10.1039/C9DT02312G

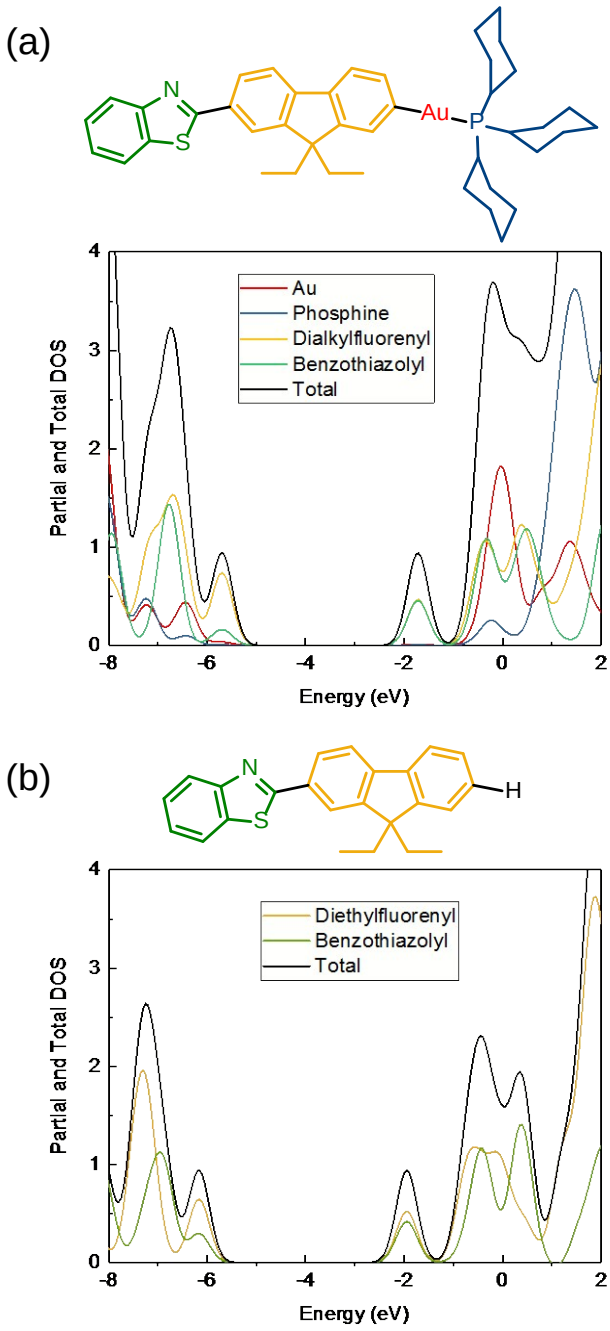

Figure 8. (a) Partial and total density-of-states plot for **AuBTF1**. (b) Partial and total density-of-states plot for unsubstituted benzothiazole-2,7-fluorene.

Figure 8 depicts a density-of-states plot of **AuBTF1** and that of the unmetallated arene. The figure shows contributions of gold, tricyclohexylphosphine, diethylfluorenyl, and benzothiazolyl moieties to the total density-of-states. Similar partitioning for the aryl ligand (where a hydrogen

View Article Online
DOI: 10.1039/C9DT02312G

atom replaces gold at carbon) is also shown. States attributable to the HOMO and LUMO derive almost wholly from the aryl ligand with little contribution from either the phosphine ligand or from gold. The LUMO is visibly separated from higher-energy orbitals, and the HOMO less so. Binding of the (phosphine)gold(I) fragment constricts the HOMO–LUMO gap: occupied orbitals are raised in energy, and vacant orbitals are lowered. Apart from this, the gross features of the ligand's density of states are retained in the complex.

These results concur with our earlier observations that (organophosphine)- and (*N*-heterocyclic carbene)gold(I) fragments are spectators that lend spin-orbit coupling to conjugated systems to which they are σ-bonded. The carbon-gold bond itself is non-chromophoric.[67,69,70,76] This observation echoes earlier results by Schanze and co-workers, who found gold(I) alkynyls to have greater linear transparency than analogous alkynyls of platinum(II).[77,78] Table I (ESI) collects results of time-dependent density-functional theory on the Franck-Condon singlet excited states of **AuBTF1**. The calculations include a continuum solvation model of toluene. The calculations find that the first excited singlet state derives (98%) from a LUMO ← HOMO excitation. The calculated transition wavelengths are in fair agreement with the absorption onset near 360 nm, Figure 2. Higher-lying singlet states are composed of multiple one-particle transitions that engage in configuration interaction.

View Article Online
DOI: 10.1039/C9DT02312G

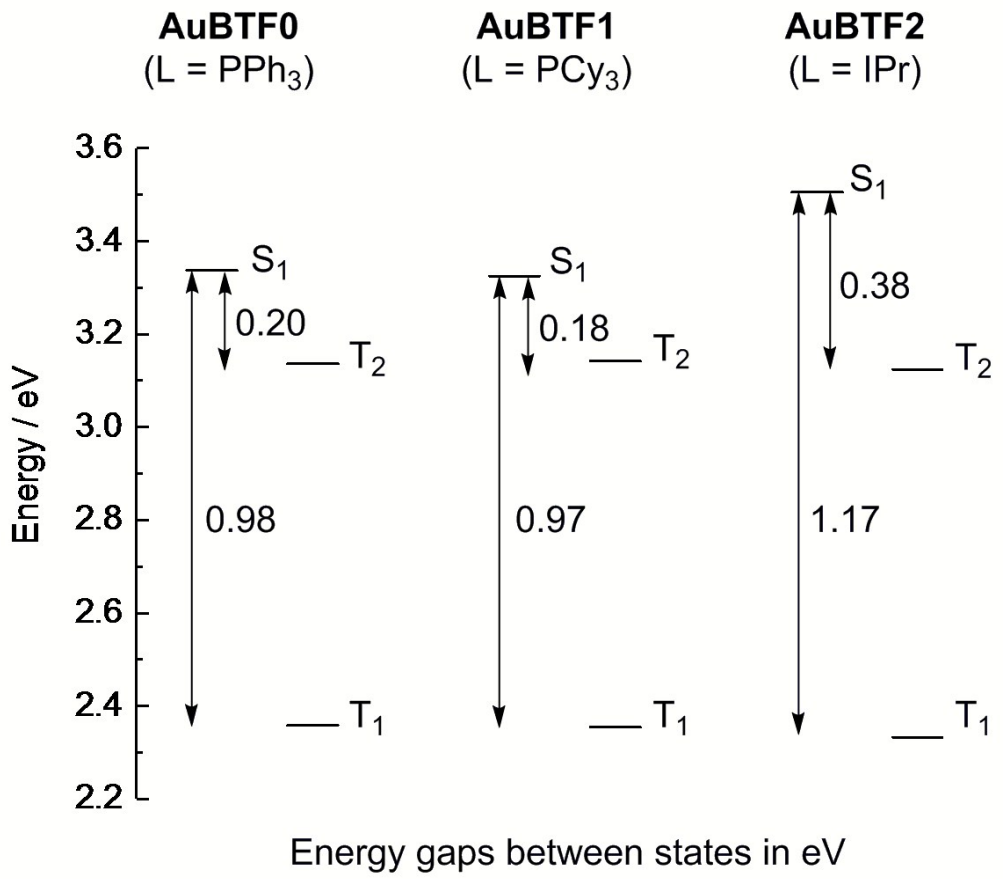

Figure 9. Time-dependent density-functional theory (TD-DFT) state plot showing S_1, T_1, and T_2 states and their corresponding energies in electron volts (eV).

Figure 9 shows a comparison of time-dependent density-functional theory (TD-DFT) state plots for all three compounds. These plots support the experimental results in which the phosphine complexes are more efficient at facilitating intersystem crossing than the carbene complex. Calculated energy gaps between the first singlet and nearest triplet state for the three compounds are consistent with faster intersystem crossing for the phosphine complexes. The carbene complex has what is essentially twice the energy gap between the S_1 and T_2 states when compared to the phosphine complexes. This is a feasible explanation for the enhanced intersystem crossing rate constants in the phosphine complexes compared to the carbene complex. Photophysical experiments comparing the rates of intersystem crossing in other organogold (I) complexes while varying the ancillary ligand from an *N*-heterocyclic carbene to an organophosphine are ongoing.

View Article Online
DOI: 10.1039/C9DT02312G

These further experimental results will provide a more thorough understanding of the nature of intersystem crossing in organogold (I) complexes.[57]

Conclusions

Three new gold(I) complexes with a benzothiazole-2,7-fluorenyl moiety bound through a gold-carbon σ-bond have been synthesized (**AuBTF0-2**). Ground-state absorption in these compounds occurs in the ultraviolet region, and all exhibit dual-luminescence following three freeze-pump-thaw cycles in toluene. The corresponding ancillary ligand (*N*-heterocyclic carbene or organophosphine) influences the excited-state dynamics of the complexes. The phosphine containing complexes, **AuBTF0** and **AuBTF1**, possess fluorescence lifetimes that are a factor of three shorter, fluorescence quantum yields that are a factor of two smaller, and intersystem crossing efficiencies that are 25 percent greater than those of the *N*-heterocyclic carbene complex, **AuBTF2**. This discrepancy in excited-state behavior has a tangible influence on the white light emission properties of the molecules. **AuBTF0** and **AuBTF1** have nearly equal fluorescence and phosphorescence quantum yields. This phenomenon leads to the observation of white light emission. For compound **AuBTF2**, the fluorescence quantum yield is higher than that of phosphorescence, resulting in a violet emission due to the enhanced contribution from the blue fluorescence. All of the AuBTF molecules have long phosphorescence lifetimes with values on the order of one ms reproduced over multiple trials. Nanosecond transient absorption spectroscopy established strong, positive triplet excited-state absorption from 400 – 800 nm for all of the derivatives. Triplet-state kinetic decay traces show laser-pulse-energy dependent behavior. Delayed fluorescence is also observed in these molecules. These observations indicate that triplet-triplet annihilation is a prominent excited-state decay pathway; the rate constant for triplet-triplet annihilation is diffusion controlled for all AuBTF molecules. Picosecond transient absorption spectroscopy at various time delays shows the evolution from the initially formed singlet excited-state to the triplet excited-state. This progression is well represented with a single exponential decay kinetic model and the presence of a single isosbestic point at ≈ 475 nm. The lifetime values obtained from fits of the picosecond transient absorption decay traces are in good agreement with the fluorescence lifetimes values obtained using TCSPC. Density-functional theory calculations support experimental observations. These calculations show that the (LUMO) and (HOMO) of

View Article Online
DOI: 10.1039/C9DT02312G

AuBTF1 are localized primarily on the aryl ligand, with a small contribution from gold in the HOMO. Time dependent-density functional calculations show that the energy gap between the S_1 and T_2 states for **AuBTF2** is almost a factor of two larger than for **AuBTF0-1**. This agrees with our excited state dynamics data that show higher intersystem crossing rate constants for **AuBTF0-1**. To our knowledge, this is the first example of single-component mononuclear gold(I) complexes exhibiting non-excimeric state white light emission, although gold(III) aryl compounds that undergo this mechanism to achieve white-light are known.[62] We are currently synthesizing and characterizing gold(I) compounds bearing the benzothiazole-2,7-fluorenyl moiety in myriad ways. These results will be reported in due course.

Acknowledgment. This work is supported by the Air Force Office of Scientific Research, contract FA9550-18-1-0247 to T. G. G. All AFRL affiliated authors recognize the Air Force Office of Scientific Research under AFOSR Award 9550-19-1-18RX056 and the Air Force Research Laboratory/RXAP contract FA8650-16-D-5402-0001. NSF is acknowledged through the Major Research Instrumentation Program under Grant No. CHE 1625543 to M. Z. (funding for the single crystal X-ray diffractometer). We thank Dr. Amanda N. Sulicz for early experimentation.

ORCID NUMBERS

J. J. Mihaly: 0000-0002-2259-0713

D. J. Stewart: 0000-0003-3246-3723

T. G. Gray: 0000-003-1756-8877

T. A. Grusenmeyer: 0000-0002-1842-056X

Electronic Supplementary Information (ESI) Available: Materials and experimental methods, synthetic details for **AuBTF0–2**, ^{1}H and ^{31}P NMR, mass spectrometry, elemental analysis, fluorescence and phosphorescence lifetime fits, fluorescence and phosphorescence quantum yield data, singlet oxygen phosphorescence quantum yield data, delayed fluorescence as a function of laser power, triplet-triplet annihilation fitting, data used to calculate excited-state extinction coefficients, ultrafast transient absorption kinetic fit data, a summary of the calculated electronic

View Article Online
DOI: 10.1039/C9DT02312G

transitions obtained from TD-DFT calculations for **AuBTF1** and **AuBTF2** and the details for X-ray crystallography data collection, work-up and experimental details for **AuBTF0** -**AuBTF2** are all included in the Supplementary Information.

Complete crystallographic data, in CIF format, have been deposited with the Cambridge Crystallographic Data Centre. CCDC 1917590-1917592 contains the supplementary crystallographic data for this paper. These data can be obtained free of charge from The Cambridge Crystallographic Data Centre via www.ccdc.cam.ac.uk/data_request/cif.

TOC Figure.

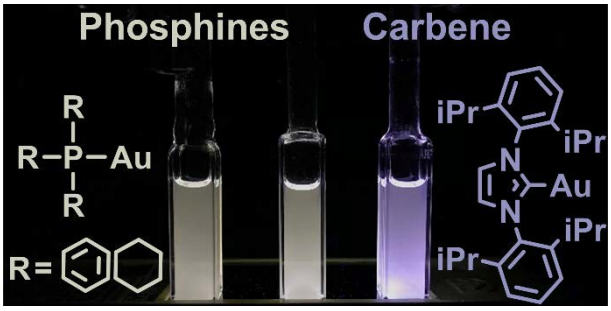

View Article Online
DOI: 10.1039/C9DT02312G

References

1 D. M. Arias-Rotondo and J. K. Mccusker, in *Visible Light Photocatalysis in Organic Chemistry*, Wiley-VCH Verlag GmbH & Co. KGaA, Weinheim, Germany, 2017, pp. 1–24.

2 E. Zysman-Colman, Ed., *Iridium(III) in Optoelectronic and Photonics Applications*, John Wiley & Sons, Ltd, Chichester, UK, 2017.

3 H. Yersin, *Highly Efficient OLEDs with Phosphorescent Materials*, Wiley-VCH Verlag GmbH & Co. KGaA, Weinheim, Germany, 2008.

4 T. Y. Li, J. Wu, Z. G. Wu, Y. X. Zheng, J. L. Zuo and Y. Pan, *Coord. Chem. Rev.*, 2018, 374, 55–92.

5 C. M. Che, C. C. Kwok, C. F. Kui, S. L. Lai and K. H. Low, in *Comprehensive Inorganic Chemistry II (Second Edition): From Elements to Applications*, Elsevier, 2013, vol. 8, pp. 607–655.

6 C. K. Prier, D. A. Rankic and D. W. C. MacMillan, *Chem. Rev.*, 2013, **113**, 5322–5363.

7 Y. You and W. Nam, *Chem. Soc. Rev.*, 2012, 41, 7061–7084.

8 K. T. Chan, G. S. M. Tong, W. P. To, C. Yang, L. Du, D. L. Phillips and C. M. Che, *Chem. Sci.*, 2017, **8**, 2352–2364.

9 G. S. Ming Tong, K. T. Chan, X. Chang and C. M. Che, *Chem. Sci.*, 2015, **6**, 3026–3037.

10 G. Di Marco, M. Lanza, M. Pieruccini and S. Campagna, *Adv. Mater.*, 1996, **8**, 576–580.

11 K. Y. Zhang, P. Gao, G. Sun, T. Zhang, X. Li, S. Liu, Q. Zhao, K. K. W. Lo and W. Huang, *J. Am. Chem. Soc.*, 2018, **140**, 7827–7834.

12 M. C. DeRosa, D. J. Hodgson, G. D. Enright, B. Dawson, C. E. B. Evans and R. J. Crutchley, *J. Am. Chem. Soc.*, 2004, **126**, 7619–7626.

13 L. Wang, H. Yin, M. A. Jabed, M. Hetu, C. Wang, S. Monro, X. Zhu, S. Kilina, S. A. McFarland and W. Sun, *Inorg. Chem.*, 2017, **56**, 3245–3259.

14 T. Huang, Q. Yu, S. Liu, W. Huang and Q. Zhao, *Dalt. Trans.*, 2018, **47**, 7628–7633.

15 D. L. Ashford, M. K. Gish, A. K. Vannucci, M. K. Brennaman, J. L. Templeton, J. M. Papanikolas and T. J. Meyer, *Chem. Rev.*, 2015, **115**, 13006–13049.

16 M. Grätzel*, , DOI:10.1021/IC0508371.

17 Y.-J. Su, H.-L. Huang, C.-L. Li, C.-H. Chien, Y.-T. Tao, P.-T. Chou, S. Datta and R.-S. Liu, *Adv. Mater.*, 2003, **15**, 884–888.

18 J. Li, P. I. Djurovich, B. D. Alleyne, M. Yousufuddin, N. N. Ho, J. C. Thomas, J. C. Peters, R. Bau and M. E. Thompson, *Inorg. Chem.*, 2005, **44**, 1713–1727.

19 M. K. Nazeeruddin, R. Humphry-Baker, D. Berner, S. Rivier, L. Zuppiroli and M. Graetzel, *J. Am. Chem. Soc.*, 2003, **125**, 8790–8797.

20 S. Lamansky, P. Djurovich, D. Murphy, F. Abdel-Razzaq, R. Kwong, I. Tsyba, M. Bortz, B. Mui, R. Bau and M. E. Thompson, *Inorg. Chem.*, 2001, **40**, 1704–1711.

21 S. Lamansky, P. Djurovich, D. Murphy, F. Abdel-Razzaq, H. E. Lee, C. Adachi, P. E. Burrows, S. R. Forrest and M. E. Thompson, *J. Am. Chem. Soc.*, 2001, **123**, 4304–4312.

22 M. A. Baldo, S. Lamansky, P. E. Burrows, M. E. Thompson and S. R. Forrest, *Appl. Phys. Lett.*, 1999, **75**, 4.

23 J. Lee, H. F. Chen, T. Batagoda, C. Coburn, P. I. Djurovich, M. E. Thompson and S. R. Forrest, *Nat. Mater.*, 2016, **15**, 92–98.

24 Y. Sun, N. C. Giebink, H. Kanno, B. Ma, M. E. Thompson and S. R. Forrest, *Nature*, 2006, **440**, 908–912.

View Article Online
DOI: 10.1039/C9DT02312G

25 H. Na, P. N. Lai, L. M. Cañada and T. S. Teets, *Organometallics*, 2018, **37**, 3269–3277.
26 W. Wei, S. A. M. Lima, P. I. Djurovich, A. Bossi, M. T. Whited and M. E. Thompson, *Polyhedron*, 2018, **140**, 138–145.
27 H. Na and T. S. Teets, *J. Am. Chem. Soc.*, 2018, **140**, 6353–6360.
28 C. Jeong, C. Coburn, M. Idris, Y. Li, P. I. Djurovich, M. E. Thompson and S. R. Forrest, *Org. Electron. physics, Mater. Appl.*, 2019, **64**, 15–21.
29 P. N. Lai, C. H. Brysacz, M. K. Alam, N. A. Ayoub, T. G. Gray, J. Bao and T. S. Teets, *J. Am. Chem. Soc.*, 2018, **140**, 10198–10207.
30 J. Lee, C. Jeong, T. Batagoda, C. Coburn, M. E. Thompson and S. R. Forrest, *Nat. Commun.*, 2017, **8**, 1–9.
31 C. Adachi, M. A. Baldo, M. E. Thompson and S. R. Forrest, *J. Appl. Phys.*, 2001, **90**, 5048–5051.
32 T. Ogawa, N. Yanai, A. Monguzzi and N. Kimizuka, *Sci. Rep.*, 2015, **5**, 10882.
33 P. Duan, N. Yanai and N. Kimizuka, *Chem. Commun.*, 2014, **50**, 13111–13113.
34 J. H. Kim, F. Deng, F. N. Castellano and J. H. Kim, *Chem. Mater.*, 2012, 24, 2250–2252.
35 D. Dini, M. J. F. Calvete and M. Hanack, *Chem. Rev.*, 2016, 116, 13043–13233.
36 G. J. Zhou and W. Y. Wong, *Chem. Soc. Rev.*, 2011, 40, 2541–2566.
37 A. Haque, R. A. Al-Balushi, I. J. Al-Busaidi, M. S. Khan and P. R. Raithby, *Chem. Rev.*, 2018, 118, 8474–8597.
38 C. L. Ho, Z. Q. Yu and W. Y. Wong, *Chem. Soc. Rev.*, 2016, 45, 5264–5295.
39 M. Tang, C. Lee, S. Lai, M. Ng, M. Chan and V. W. Yam, *J. Am. Chem. Soc.*, 2017, **139**, 9341–9349.
40 F. K. Kong, M. Tang, Y. Wong, M. Chan and V. W. Yam, , DOI:10.1021/jacs.6b02632.
41 V. W. Yam, 2014, 17861–17868.
42 V. K. Au, K. M. Wong, D. P. Tsang, M. Chan, N. Zhu and V. W. Yam, 2010, 14273–14278.
43 E. Studies, V. K. Au, D. P. Tsang, K. M. Wong, M. Chan, N. Zhu and V. W. Yam, , DOI:10.1021/ic4019212.
44 V. W. Yam, 2018, 6228–6232.
45 A. Y. Tam, D. P. Tsang, M. Chan, N. Zhu and V. W. Yam, 2011, 3383–3385.
46 K. M. Wong, X. Zhu, L. Hung, N. Zhu, V. W. Yam and H. Kwok, 2005, **2**, 2906–2908.
47 L. Li, M. Tang, W. Cheung, S. Lai, M. Ng, C. K. Chan, M. Chan and V. W. Yam, , DOI:10.1021/acs.chemmater.9b01208.
48 D. P. K. Tsang, M. Y. Chan, A. Y. Y. Tam and V. W. W. Yam, *Org. Electron. physics, Mater. Appl.*, 2011, **12**, 1114–1119.
49 G. Zhou, Q. Wang, X. Wang, C. L. Ho, W. Y. Wong, D. Ma, L. Wang and Z. Lin, *J. Mater. Chem.*, 2010, **20**, 7472–7484.
50 S. Fuertes, A. J. Chueca, M. Perálvarez, P. Borja, M. Torrell, J. Carreras and V. Sicilia, *ACS Appl. Mater. Interfaces*, 2016, **8**, 16160–16169.
51 Y. Uchida, *Opt. Eng.*, 2006, **44**, 124003.
52 L. M. Huang, G. M. Tu, Y. Chi, W. Y. Hung, Y. C. Song, M. R. Tseng, P. T. Chou, G. H. Lee, K. T. Wong, S. H. Cheng and W. S. Tsai, *J. Mater. Chem. C*, 2013, **1**, 7582–7592.
53 B. W. D'Andrade, J. Brooks, V. Adamovich, M. E. Thompson and S. R. Forrest, *Adv. Mater.*, 2002, **14**, 1032.
54 H. J. Bolink, F. De Angelis, E. Baranoff, C. Klein, S. Fantacci, E. Coronado, M. Sessolo, K. Kalyanasundaram, M. Grätzel and M. K. Nazeeruddin, *Chem. Commun.*, 2009, 4672–

View Article Online
DOI: 10.1039/C9DT02312G

4674.
55 *Green Energy and Technology*, 2012.
56 S. Reineke, M. Thomschke, B. Lüssem and K. Leo, *Rev. Mod. Phys.*, 2013, **85**, 1245–1293.
57 Y. Chang, K. Tang, H. Pan, S. Liu, I. O. Koshevoy, A. J. Karttunen, W. Hung, M. Cheng and P. Chou, *J. Phys. Chem. C* **2013**, 9623–9632 DOI:10.1021/jp402666r.
58 J. Jiang, Y. Xu, W. Yang, R. Guan, Z. Liu, H. Zhen and Y. Cao, *Adv. Mater.*, 2006, **18**, 1769–1773.
59 H. Zhen, W. Xu, W. Yang, Q. Chen, Y. Xu, J. Jiang, J. Peng and Y. Cao, *Macromol. Rapid Commun.*, 2006, **27**, 2095–2100.
60 M. Bachmann, D. Suter, O. Blacque and K. Venkatesan, *Inorg. Chem.*, 2016, **55**, 4733–4745.
61 W. X. Ni, M. Li, J. Zheng, S. Z. Zhan, Y. M. Qiu, S. W. Ng and D. Li, *Angew. Chemie - Int. Ed.*, 2013, **52**, 13472–13476.
62 M. Bachmann, O. Blacque and K. Venkatesan, *Chem. - A Eur. J.*, 2017, **23**, 9451–9456.
63 B. Zhang, Y. Li, R. Liu, T. M. Pritchett, A. Azenkeng, A. Ugrinov, J. E. Haley, Z. Li, M. R. Hoffmann and W. Sun, *Chem. - A Eur. J.*, 2012, **18**, 4593–4606.
64 H. K. Lenker, T. G. Gray and R. A. Stockland, *Dalt. Trans.*, 2012, **41**, 13274–13276.
65 D. V. Partyka, M. Zeller, A. D. Hunter and T. G. Gray, *Inorg. Chem.*, 2012, **51**, 8394–8401.
66 D. V. Partyka, T. S. Teets, M. Zeller, J. B. Updegraff, A. D. Hunter and T. G. Gray, *Chem. - A Eur. J.*, 2012, **18**, 2100–2112.
67 L. Gao, M. A. Peay, D. V. Partyka, J. B. Updegraff, T. S. Teets, A. J. Esswein, M. Zeller, A. D. Hunter and T. G. Gray, *Organometallics*, 2009, **28**, 5669–5681.
68 D. V. Partyka, J. B. Updegraff, Z. M. Matthia, A. D. Hunter and G. Thomas, *Organometallics*, 2009, **28**, 1666–1674.
69 D. V. Partyka, M. Zeller, A. D. Hunter and T. G. Gray, *Angew. Chemie - Int. Ed.*, 2006, **45**, 8188–8191.
70 L. Gao, D. S. Niedzwiecki, N. Deligonul, M. Zeller, A. D. Hunter and T. G. Gray, *Chem. - A Eur. J.*, 2012, **18**, 6316–6327.
71 K. A. Porter, A. Schier and H. Schmidbaur, *Organometallics*, 2003, **22**, 4922–4927.
72 L. Gao, M. A. Peay, D. V. Partyka, J. B. Updegraff, T. S. Teets, A. J. Esswein, M. Zeller, A. D. Hunter and T. G. Gray, *Organometallics*, 2009, **28**, 5669–5681.
73 J. R. Lakowicz, *Principles of Fluorescece Spectroscopy*, Springer US, 3rd Editio., 2006.
74 M. Montalti, A. Credi, L. Prodi and M. Teresa Gandolfi, *Handbook of Photochemistry, Third Edition*, CRC Press, 3rd Editio., 2006.
75 T. N. Singh-Rachford and F. N. Castellano, *Coord. Chem. Rev.*, 2010, **254**, 2560–2573.
76 D. V. Partyka, A. J. Esswein, M. Zeller, A. D. Hunter and T. G. Gray, *Organometallics*, 2007, **26**, 3279–3282.
77 S. Goswami, G. Wicks, A. Rebane and K. S. Schanze, *Dalt. Trans.*, 2014, **43**, 17721–17728.
78 S. Goswami, R. W. Winkel and K. S. Schanze, *Inorg. Chem.*, 2015, **54**, 10007–10014.